Combinatorial Optimization of $(Y_xLu_{1-x-y})_3Al_5O_{12}:Ce_{3y}$ Green-Yellow Phosphors

Kong Zhang,[†,‡] Qingfeng Liu,[†] Qian Liu,*[,†] Yun Shi,[§] and Yubai Pan[§]

The State Key Laboratory of High Performance Ceramics and Superfine Microstructure, Shanghai Institute of Ceramics, Chinese Academy of Sciences, Shanghai 200050, China, Graduate University of the Chinese Academy of Sciences, Beijing 100049, China, and Key Laboratory of Transparent Opto-functional Inorganic Material, Shanghai Institute of Ceramics, Chinese Academy of Sciences, Shanghai 200050, China

Received January 12, 2010

A combinatorial chemistry method was used to synthesize and screen $(Y_xLu_{1-x-y})_3Al_5O_{12}:Ce_{3y}$ green-yellow phosphors. The material libraries were obtained using an inkjet delivery system and screened for their fluorescence under an ultraviolet light of 365 nm. The optimized composition was identified to be $(Y_{0.2}Lu_{0.788})_3Al_5O_{12}:Ce^{3+}_{0.036}$. Scale-up experiments confirmed that the optimized composition of the phosphor showed the highest luminescence intensity and an excellent scintillation performance with a short decay time (<60 ns). The results indicated that the $(Y_xLu_{1-x-y})_3Al_5O_{12}:Ce_{3y}$ could be potentially useful as green-yellow phosphors for ceramic scintillators.

Introduction

Scintillators play an important role in detecting high energy photons and particles, which are widely used in medical diagnostic imaging and industrial measuring systems.[1] Recently, materials based on the garnet structure ($Y_3Al_5O_{12}$) are promising candidates for scintillators applications for their high energy-efficiency, high reliability, long life, fast response, and easy doping of rare-earth elements. And the Ce-doped $Y_3Al_5O_{12}$ (YAG:Ce) and $Lu_3Al_5O_{12}$ (LuAG:Ce) are the most studied garnet materials for scintillators in previous reports.[2−4] Unfortunately, YAG:Ce is deficient in stopping power because of its low density, and the restriction concerning the LuAG:Ce is that the high purity Lu_2O_3 starting powders are expensive from an industrial point of view. So the Ce-doped dual-element mixed composition of YLuAG single crystals with the same garnet-type structure have attracted much attention in laser applications. But this kind of single crystals is almost entirely grown from the melt by slow cooling in an iridium crucible, so they are still very expensive, and it is difficult to produce large-sized single crystals.[5] As an alternative, polycrystalline ceramic scintillators of YLuAG:Ce are considered and studied for its convenient ceramic processing techniques and analogous scintilla performance. Following this is a systematical study of the optimal replacement effect of Y for Lu, and also of the effect of Ce doping necessary to realize the best luminescence.

To enhance the efficiency and raise the speed of the time-consuming systematic search of YLuAG:Ce, the combinational chemistry method is used in this paper. As is well-known, the combinatorial chemistry method has been widely applied to the synthesis of various materials, such as drugs in pharmaceutical analysis, phosphors, catalysts, and so forth, owing to its accelerated rate of finding new target materials by the rapid synthesis and characteration of large libraries. As for the phosphor libraries, they can be synthesized in either thin-film or powder forms.[6−10] In the synthesis of powder-form libraries, the solutions of elemental precursors are delivered using an automatic liquid injector with an accurate control of elements mix in an array of cells.[11−13]

To achieve a high density and transparency of ceramic scintillator, we choose $(Y_xLu_{1-x-y})_3Al_5O_{12}:Ce_{3y}$ (YLuAG:Ce) as the phosphors composition in present research. The luminescence of YLuAG:Ce phosphors can be strongly affected by the energy transfer process from the host to activator. The host condition depends on the proportion of Y and Lu which is designed by the variety of *x*. And the doped concentration of Ce designed by the variety of *y* is also a key factor which influences the energy transfer. In this regard, there are a large potential number of solid solutions for the $(Y_xLu_{1-x-y})_3Al_5O_{12}:Ce_{3y}$ composition system. So the combinatorial chemistry method of adopting an inkjet delivery system was used to synthesize in parallel composition libraries of $(Y_xLu_{1-x-y})_3Al_5O_{12}:Ce_{3y}$ phosphors.

And the libraries were rapidly screened under the UV photoluminescence. The optimum composition of this phosphor was reproduced by a nitrate pyrogenation synthesis under the same experimental conditions to obtain bulk samples, and these bulk samples were analyzed in detail to

* To whom correspondence should be addressed. E-mail: qianliu@sunm.shcnc.ac.cn. Phone: +86 021 52412612. Fax: +86 021 52413122.
† The State Key Laboratory of High Performance Ceramics and Superfine Microstructure, Shanghai Institute of Ceramics.
‡ Graduate University of the Chinese Academy of Sciences.
§ Key Laboratory of Transparent Opto-functional Inorganic Material, Shanghai Institute of Ceramics.

10.1021/cc1000055 © 2010 American Chemical Society
Published on Web 05/18/2010

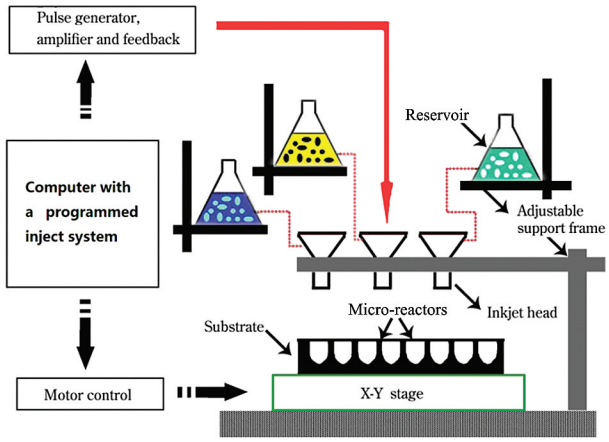

Figure 1. Schematic diagram of the drop-on-demand inkjet delivery system for YLuAG:Ce library preparation (refs 14, 15).

Table 1. Details about the Solutions Used in Precursor Delivery

raw material	purity	solution	concentration
$Al(NO_3)_3$	AR	deionized water	1 M
$Ce(NO_3)_3$	AR	deionized water	0.05 M
Y_2O_3	99.99%	10% HNO_3	1 M
Lu_2O_3	99.99%	20% HNO_3	1 M

obtain the information of structure, morphology, photoluminescence, and scintillation performance.

Experimental Section

YLuAG:Ce material libraries were designed in a combinatorial approach and prepared using an inkjet delivery system (model-CIJ fabricated by the University of Science and Technology (USTC) of China, Hefei, China). The schematic diagram of the inkjet delivery system is shown in Figure 1. The eight independent piezoelectric inkjet heads and the X−Y stage are controlled by the computer via the driving circuit and motor controller. Each inkjet head is connected to a solution reservoir through a tube, and a sintered alumina plate substrate with some cells was used to hold liquid precursors for powder phosphors. The neighboring cells are 3 mm in center to center separation, and the alumina substrate is fixed on the stage. More details can be found in some published reports written by Gao et al. of USTC.[14,15]

To keep a small composition step controllable, Al and Ce solutions were prepared by dissolving $Al(NO_3)_3 \cdot 9H_2O$ (A.R) and $Ce(NO_3)_3 \cdot 6H_2O$ (A.R) in deionized water. Y and Lu solutions were prepared by dissolving Y_2O_3 and Lu_2O_3 (all 99.99%) in nitric acid (A.R). The details about the solutions used in the precursor delivery are summarized in Table 1. Before ejection, the solutions were infused with argon gas for 3 h to expel any air dissolved in the suspension which has a tendency to agglomerate and block the nozzle. Then the accurate amount of each solution was collected in the microreactors with the assistance of a computer programmed injection system according to the composition map. The solutions in the microreactors were agitated in an ultrasonic bath for 2 h and then dried at 80 °C for 24 h. Most of the solution turned into a gel state at this stage and then calcined at 600 °C for 4 h. These samples were subsequently heat treated at 800 °C−1400 °C for complete calcination in a weak reduced atmosphere. Then the prepared library was excited with a Hg UV lamp with a 365 nm broadband filter, and the photoluminescent intensity of the small samples in the library was recorded using a digital CCD camera.

After the first combinatorial screening process, we take the preferable area in the compositional map of the powder phosphor library for a new design with a smaller compositional interval. Thereafter, a high-throughput synthesis and screening were implemented as the first screen. Through this two-step combinatorial process, the optimization compositions were confirmed. Then a conventional nitrate- pyrogenation was used to synthesize a larger amount of powders for sintering bulk samples for a further investigation. The powder phase and crystal structure were identified by X-ray diffraction analysis (D/max 2550 V). The powder morphology and dispersity were observed using a field emission scanning electron microscope (JSM-6700F FESEM). And the excitation and emission spectra were obtained on a luminescence spectrometer (Hitach, F-4600) at room temperature. The decay time was measured on a FLS920 spectrometer.

Results and Discussion

Figure 2 presents the composition maps, a 9 × 9 array and a 6 × 9 array, and luminescent photographs of $(Y_xLu_{1-x-y})_3Al_5O_{12}:Ce_{3y}$ libraries obtained under 365 nm UV excitation. The powder samples on the chip were all calcined under the optimal condition of 1000 °C for 2 h.The lamp light was illuminated evenly over the library, so that a relative comparison could be made among the samples in the library. Figure 2a shows the first screen results with a 9 × 9 array with different Y contents from $x = 0.1$ to 0.9 and Ce^{3+} doping contents from $y = 0.01$ to 0.09. It is obvious that the brighter luminescent composition points appear on the top left area of the composition map, for example the points (1,1), (1,2), (2,1), (2,2), (4,1), (4,2) in the 9 × 9 array. From the Figure 2a, we can find that the intensities rapidly decrease when the replacement content of Y exceeds 0.6. Taking a transverse contrast, the concentration quenching is also observed with the Ce content exceeding ∼4%, which is the same as the previous report,[16] only for the compositions of lower Y replacement (x = 0.1 or 0.2). To zoom in on the higher luminescent region, a secondary combinatorial design was implemented with smaller composition steps. This process yielded another new library with a 6 × 9 array with the Y contents from $x = 0.1$ to 0.6 and Ce contents from $y = 0.003$ to 0.027. The 365 nm UV photoluminescent photograph and composition map are shown in Figure 2b, where the highest UV photoluminescent compositions are found at $x = 0.2$, $y = 0.006-0.012$, that are the points of (2,2), (2,3), (2,4) in the 6 × 9 array.

To confirm the above results and get more particular information of the screened composition, some scale-up samples for $(Y_xLu_{1-x-y})_3Al_5O_{12}:Ce_{3y}$ were synthesized through a nitrate pyrogenation reaction under the same conditions as the libraries preparation parameters. Figure 3a shows the X-ray diffraction (XRD) patterns of powder sample $Y_{0.600}Lu_{2.364}Al_5O_{12}:Ce_{0.036}$ ($x = 0.2$, $y = 0.012$) that is one of the optimized compositions based on the secondary screening,

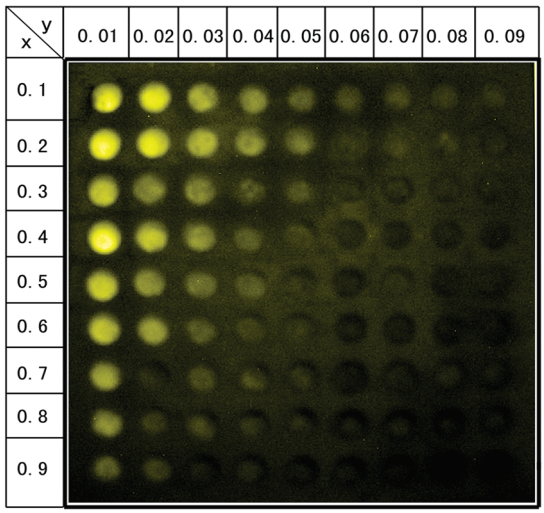

(a)

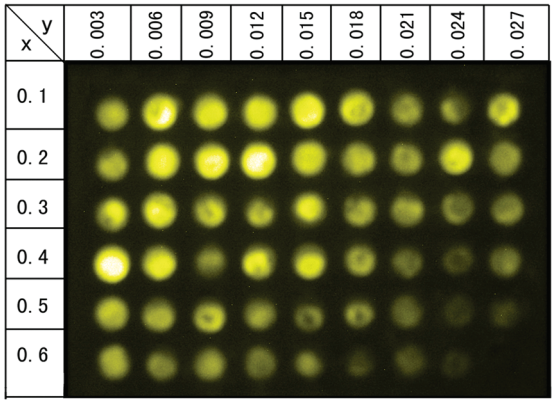

(b)

Figure 2. Composition map and photoluminescence photography of the libraries excited under 365 nm UV light for $(Y_xLu_{1-x-y})_3Al_5O_{12}$:$Ce_{3y}$, (a) the first screen (b) the second screen.

after calcination in a weak reduce ambience at 800 °C, 1000 °C, 1300°, along with the standard XRD spectra of YAG and LuAG as well. An ideal crystal structure of YLuAG:Ce garnet is also shown in the Figure 3b, together with the structural parameters given in Table 2. The observed peaks in the XRD spectra can be indexed on the basis of a cubic unit cell (space group *Ia*3*d*), which proves that the prepared powder has a same garnet structure as YAG and LuAG. Compared with standard phase of YAG (JCPDS card #72−1853) and LuAG (JCPDS card #73−1368), there is no other phase present in the patterns. Figure 3c shows a scanning electron microscopy (SEM) picture of the powder morphology, produced with the nitrate pyrogenation reaction, after calcination at 1000 °C. From the picture, it is noticed that there are many large particles which were composed of primary particles. These primary particles are nanosized and bridged by hydrogen bonds and the huge capillary force.

Excitation (λ_{em} = 540 nm) and emission (λ_{ex} = 448 nm) spectra of $(Y_xLu_{1-x-y})_3Al_5O_{12}$:$Ce_{3y}$ phosphors measured at room temperature are shown in Figure 4. The compositions design of the two groups of scale-up samples are corresponding to the content variety of either doping Ce^{3+} (x = 0.2; y = 0.009, 0.012, 0.015) or replacement of Y (y = 0.012;

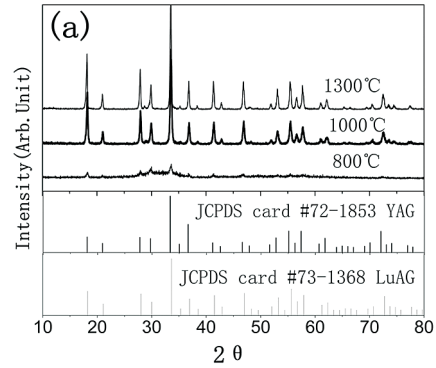

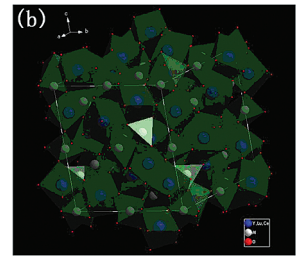

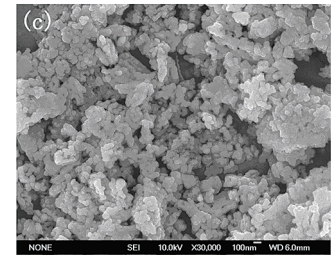

Figure 3. (a) XRD patterns of $(Y_xLu_{1-x-y})_3Al_5O_{12}$:$Ce_{3y}$ (x = 0.2, y = 0.012) powders after calcination at 800 °C, 1000 °C, 1300°, along with the standard XRD spectra of YAG and LuAG. (b) An ideal garnet crystal structure of YLuAG:Ce, (c) SEM morphology of $(Y_xLu_{1-x-y})_3Al_5O_{12}$:$Ce_{3y}$ (x = 0.2, y = 0.012) powders after calcination at 1000 °C.

Table 2. Ideal Crystallographic Data for $(Y_xLu_{1-x-y})_3Al_5O_{12}$:$Ce_{3y}$ (x = 0.2, y = 0.012) Phosphor, Constraints on Atomic Position, and U_{iso}

	Wyckoff site	*x*/*a*	*y*/*b*	*z*/*c*	occupancy	*U* [Å^2]
Y	24c	1/8	0	1/4	0.600	0.0051
Lu	24c	1/8	0	1/4	2.364	0.0051
Ce	24c	1/8	0	1/4	0.036	0.0051
Al_1	16a	0	0	0	2	0.0042
Al_2	24d	3/8	0	1/4	3	0.0023
O	96h	0.28020	0.10120	0.19930	12	0.0048

x = 0.10, 0.15, 0.20, 0.25, 0.30), where the composition points (x = 0.2, y = 0.009−0.015) are the brighter points on the secondary screening. It can be noticed that both the shape and position of the excitation spectra from the Ce^{3+} emission at 540 nm (Figure 4a, c) show no obvious changes with the difference of Y and Ce concentrations. But, for the group one of the scale-up sample (x = 0.2; y = 0.009, 0.012, 0.015) the lowest peak intensity is from the sample of $Y_{0.6}Lu_{2.375}Al_5O_{12}$:$Ce_{0.027}$ with a lowest Ce^{3+} dopant concentration, that is, the sample x = 0.2, y = 0.009. It is obvious that the result is coincident with our second screen of combinatorial research between the compositions of x = 0.2, y = 0.009−0.015 (Figure 2b). Comparatively, for the group two of the scale-up sample (y = 0.012; x = 0.10, 0.15, 0.20, 0.25, 0.30), the strongest enhancement of excitation intensity is observed in the sample of $Y_{0.6}Lu_{2.364}Al_5O_{12}$:$Ce_{0.036}$ with a middle-level of Y replaced, that is the composition of x = 0.2, y = 0.012. Besides, the two excitation bands of both a and c spectra, namely, a weak band with a maximum at 345 nm and a strong broad band ranging from 400 nm to 500 nm with a maximum at 448 nm, were due to the electron transition from 4f ground state ($^2F_{5/2}$, $^2F_{7/2}$) of Ce^{3+} to the different crystal field splitting components of the excited 5d state. The emission spectra under 448 nm excitation (Figure

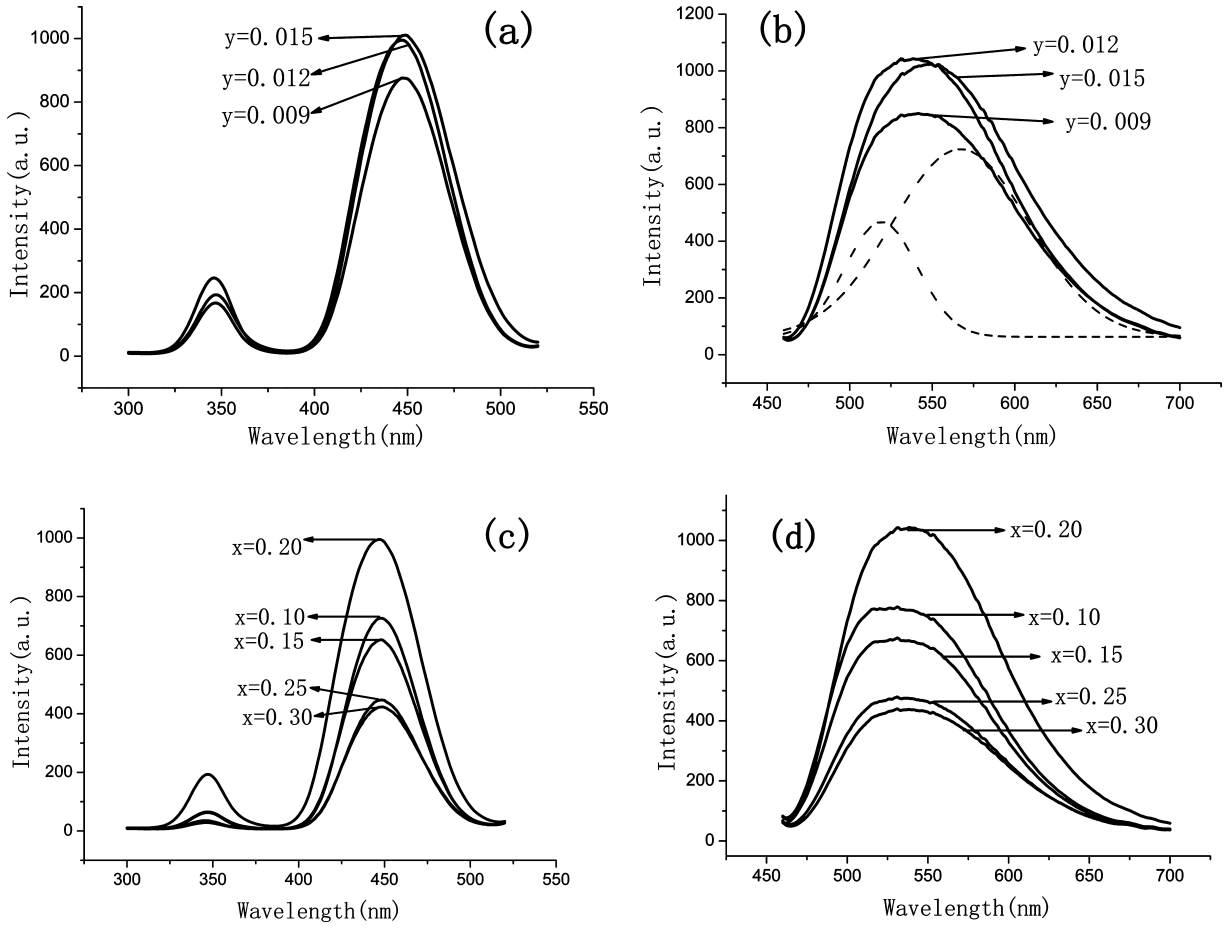

Figure 4. Excitation (a, c; $\lambda_{em} = 540$ nm) and emission (b, d; $\lambda_{ex} = 448$ nm) spectrum of $(Y_xLu_{1-x-y})_3Al_5O_{12}:Ce_{3y}$ phosphors with different Ce^{3+} and Y contents (a, b for the composition of $x = 0.2$, $y = 0.009$, 0.012, 0.015. c, d for the composition of $y = 0.012$, $x = 0.10$, 0.15, 0.20, 0.25, 0.30).

4b, d) consist of a broad band covering from 470 nm to 600 nm with a maximum at about 540 nm. According to the Gaussian fitted results, as shown in the Figure 4b (dotted line), it can be seen that the photoluminescent spectra can be deconvolved into two components centered at about 520 and 570 nm. Obviously, the emissions are ascribed to the electron transitions from the lowest crystal field-splitting component of 5d level to the 4f ground state of Ce^{3+} ($^2F_{5/2}$, $^2F_{7/2}$), respectively. It is worth to note that the lowest intensity of emission is also belongs to the samples $Y_{0.6}Lu_{2.375}Al_5O_{12}$:$Ce_{0.027}$ ($x = 0.2$, $y = 0.009$) which has a lowest intensity of excitation (Figure 4a). Similarly, the highest peak of emission is also observed in the sample of $Y_{0.6}Lu_{2.364}Al_5O_{12}:Ce_{0.036}$ ($x = 0.2$, $y = 0.012$) with a strongest enhancement of excitation (Figure 4b, 4d).

It should be noticed that the shapes of the photoluminescent spectra shows a little change with the variety of both Ce and Y composition (Figure 4b,d). However, the peak position of the emission spectra changes markedly with the variety of Ce content (Figure 4b). This shift maybe comes from the different probability of the radiative transition from 5d to the $^2F_{7/2}$ and $^2F_{5/2}$ of Ce^{3+} in these three samples as the reasons that raise the two peaks shown in Figure 4a. We suppose that this difference reflects some influences from the variation of defects in the powders, both in terms of their population and distribution.

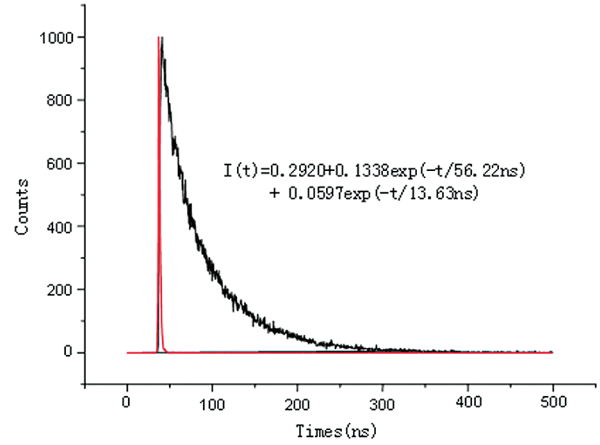

Figure 5. Photoluminescence decay of the leading visible emission of $(Y_xLu_{1-x-y})_3Al_5O_{12}:Ce_{3y}$ ($x = 0.2$, $y = 0.012$), $\lambda_{ex} = 460$ nm, $\lambda_{em} = 550$ nm. Two-exponential approximation $I(t)$ yields a long decay time of 56.22 ns, with a short decay time of 13.63 ns.

Figure 5 shows the photoluminescence decay curve for 5d→4f transition of Ce^{3+} in $Y_{0.6}Lu_{2.364}Al_5O_{12}:Ce_{0.036}$ ($x = 0.2$, $y = 0.012$, an optimal composition with the highest emission peak) powder at room temperature. The curve could be fitted by a two-exponential approximation function with a long decay time of about 56.22 ns (the value is close to the intrinsic decay time ~60 ns of YAG:Ce at 300 K)[17] and a short decay time of about 13.63 ns. Generally speaking, there are two paths for the excited state to relax to the ground

state, namely, the radiative process with emission of photons and the non-radiative process.[18] Therefore, the lifetime can be described by the rate equation qualitatively as

$$\tau = (\gamma_r + \gamma_{nr})^{-1},$$

where γ_r is the radiative rate and γ_{nr} is the non-radiative rate.[19,20] Generally, the Cerium ions which are located in the bulk phase of the powders most likely occupy the positions similar to the ones of Ce^{3+} sited in the bulk material (e.g., single crystal), and the energy transfer to the quenching centers is negligible, that is, the non-radiative process is negligible. Therefore, the long decay time (~56 ns, in the present work) is mainly related to the conventional emission of photons from bulk phase. But thinking of the considerable surface areas of nanosized phosphors powders prepared, definitely, there are many defects on the surface layer of powders, which act as the quenching centers of luminescence. So, the energy transfer from the excited Ce^{3+} on the surface to these quenching centers is much more severe than this kind of energy transfer process in the bulk phase. Then the non-radiative rate (γ_{nr}) related to this surface quenching increases markedly, and the lifetime τ turns shorter accordingly. So the short decay time (~14 ns, in the present work) expresses the photoluminescence decay of Ce^{3+} on the special positions coming from the interaction between the excited Ce^{3+} on the surface and surface defects.[21−23] The optical mechanism of photoluminescence decay will be studied in our following work and discussed in another paper. Both the emission spectra and photoluminescence decay curve also indicate that the sample with an optimum composition $(Y_{0.2}Lu_{0.788})_3Al_5O_{12}:Ce^{3+}_{0.036}$ can be a promising material for scintillators, having a higher emission and a shorter decay time.

Conclusion

The green-yellow phosphors of $(Y_xLu_{1-x-y})_3Al_5O_{12}:Ce_{3y}$ material libraries were synthesized and screened by using the combinatorial chemistry method. The optimum composition was found to be $(Y_{0.2}Lu_{0.788})_3Al_5O_{12}:Ce^{3+}_{0.036}$, with the strongest intensity of emission under 448 nm. And also the scale-up powder samples with optimal composition were synthesized through a nitrate pyrogenation reaction under the same preparation condition as the libraries to confirm the combinatorial optimization. The highest peak of emission is also observed in the synthesized powder sample of $Y_{0.6}Lu_{2.364}Al_5O_{12}:Ce_{0.036}$ ($x = 0.2$, $y = 0.012$) with a strongest enhancement of excitation. It is the powder that has a long decay time of about 56.22 ns (close to the intrinsic decay time ~60 ns of YAG:Ce at 300 K) and a short decay time of about 13.63 ns. On the basis of the results, it is reasonable to believe that the combinatorial chemistry screening has a high efficiency for finding a new green-yellow phosphor as a candidate of ceramic scintillator materials.

Acknowledgment. This work is financially supported by the National High Technology Research and Development Program of China (863 Program, No. 2009AA03Z437) and Science & Technology Commission of Shanghai Municipality (No.O8JC1420500). The authors also thank The State Key Laboratory of High Performance Ceramics and Superfine Microstructure, Shanghai Institute of Ceramics, for providing help with the sample preparation and testing.

References and Notes

(1) Li, H. L.; Liu, X. J.; Xie, R. J.; Zhou, G. H.; Naoto, H.; Pu, X. P.; Huang, L. P. *Jpn. J. Appl. Phys.* **2008**, *47*, 1657–1661.
(2) Zorenko, Y.; Gorbenko1, V.; Voloshinovskii, A.; Stryganyuk, G.; Mikhailin, V.; Kolobanov, V.; Spassky, D.; Nikl, M.; Blazek, K. *Phys. Status Solidi* **2005**, *202*, 1113–1119.
(3) Li, H. L.; Liu, X. J.; Huang, L. P. *J. Am. Ceram. Soc.* **2005**, *88*, 3226–3228.
(4) Yang, X. B.; Li, H. J.; Bi, Q. Y.; Su, L. B.; Xu, J. *J. Cryst. Growth.* **2009**, *311*, 3692–3696.
(5) Mihóková, E.; Nikl, M.; Mareš, J. A.; Beitlerová, A.; Vedda, A.; Nejezchleb, K.; Blaek, K.; Ambrosio, C. *J. Lumin.* **2007**, *126*, 77–80.
(6) Chan, T. S.; Liu, Y. M.; Liu, R. S. *J. Comb. Chem.* **2008**, *10*, 847–850.
(7) Chen, L.; Fu, Y. B.; Zhang, G. B.; Bao, J.; Gao, C. *J. Comb. Chem.* **2008**, *10*, 401–404.
(8) Kulshreshtha, C.; Sharma, A. K.; Sohn, K. S. *J. Comb. Chem.* **2008**, *10*, 421–425.
(9) Sharma, A. K.; Kulshreshtha, C.; Sohn, K.; Sohn, K. S. *J. Comb. Chem.* **2009**, *11*, 131–137.
(10) Sohn, K. S.; Park, D. H.; Cho, S. H.; Kim, B. I.; Woo, S. I. *J. Comb. Chem.* **2006**, *8*, 44–49.
(11) Xiang, X. D.; Sun, X. D.; Briceno, G.; Lou, Y. L.; Wang, K. A.; Chang, H.; Wallace, W.; Chen, S. W.; Schultz, P. *Science.* **1995**, *268*, 1738–1740.
(12) Briceno, G.; Chang, H.; Sun, X. D.; Schultz, P.; Xiang, X. D. *Science* **1995**, *270*, 273–275.
(13) Sun, X. D.; Wang, K. A.; Yoo, Y.; Wallace, W.; Gao, C.; Xiang, X. D.; Schultz, P. *Adv. Mater.* **1997**, *9*, 1046.
(14) Chen, L.; Bao, J.; Gao, C.; Huang, S. X.; Liu, C. H.; Liu, W. H. *J. Comb.Chem.* **2004**, *6*, 699–702.
(15) Chan, T. S.; Kang, C. C.; Liu, R. S.; Chen, L.; Liu, X. N.; Ding, J. J.; Bao, J.; Gao, C. *J.Comb. Chem* **2007**, *9*, 343–346.
(16) Katelnikovasa, A.; Vitta, P. k.; Pobedinskas., P.; Tamulaities, G.; Zukauskas, A.; Jorgensen, J. E.; Kareiva, A. *J. Cryst. Growth.* **2007**, *304*, 361–368.
(17) Weber, M. J. *Solid State Commun.* **1973**, *12*, 741–744.
(18) Zhang, K.; Liu, H. Z.; Wu, Y. T. *J. Alloys Compd.* **2008**, *453*, 265–270.
(19) Guo, H.; Yin, M.; Dong, N.; Xu, M.; Lou, L. R.; Zhang, W. P. *Appl. Surf. Sci.* **2005**, *243*, 245–250.
(20) Zhang, W. W.; Zhang, W. P.; Xie, P. B.; Yin, M.; Chen, H. T.; Jing, L.; Zhang, Y. S.; Lou, L. R.; Xia, S. D. *J. Colloid Interface Sci.* **2003**, *262*, 588–593.
(21) Pankratov, V.; Grigorjeva, L.; Millers, D.; Chudoba, T. *Radiat. Meas.* **2007**, *42*, 679–682.
(22) Tian, L. J.; Sun, Y. J.; Yu, Y.; Kong, X. G.; Zhang, H. *Chem. Phys. Lett.* **2008**, *452*, 188–192.
(23) Pankratov, V.; Grigorjeva, L.; Millers, D.; Chudoba, T.; Fedyk, R.; Lojkowski, W. *Solid State Phenom.* **2007**, *128*, 173–178.

CC1000055